A Novel Scalable Energy-Efficient Synaptic Device: Crossbar Ferroelectric Semiconductor Junction

M. Si[1], Y. Luo[2], W. Chung[1], H. Bae[1], D. Zheng[1], J. Li[1], J. Qin[1], G. Qiu[1], S. Yu[2], and P. D. Ye[1,*]
[1]School of Electrical and Computer Engineering, Purdue University, West Lafayette, IN, USA, *Email: yep@purdue.edu
[2]School of Electrical and Computer Engineering, Georgia Institute of Technology, Atlanta, GA, USA

***Abstract*—**A novel ferroelectric semiconductor junction (FSJ) based two-terminal memristor is demonstrated as a synaptic device for the first time. In this novel FSJ device, a metal-ferroelectric semiconductor (FS)-metal crossbar structure is used, instead of a metal-ferroelectric insulator-metal structure for a conventional ferroelectric tunnel junction (FTJ), so that an ultra-thin ferroelectric insulator is not required. Meanwhile, the FSJ also offers energy efficiency advantage over the conventional filament-based resistive random access memory (RRAM) device because the conductance of the FSJ scales with the junction area. Experimentally, a ferroelectric semiconductor α-In_2Se_3 based crossbar FSJ (c-FSJ) as a synaptic device is demonstrated. Ferroelectric resistive switching is clearly observed in both planar FSJ (p-FSJ) by in-plane polarization switching and c-FSJ by out-of-plane polarization switching. Conductance potentiation and depression in the c-FSJ are measured and benchmarked at both original size and projected to 32 nm node with different synaptic devices. α-In_2Se_3 c-FSJ shows good on-line learning accuracy (~92 %), low latency and energy consumption due to the short write pulse width and large R_{ON}.

I. Introduction

Emerging non-volatile memory (e-NVM) is considered as one of the promising devices for non-von Neumann computing because it can store the synaptic weights using its multiple conductance states and at the same time performs matrix multiplication and addition on-chip without accessing external memory [1, 2]. There have been reports that employed RRAM [3-6], phase change memory (PCM) [7-9], ferroelectric tunnel junction (FTJ) [10] and ferroelectric field-effect transistor (Fe-FET) [11-13] as synaptic devices for crossbar or pseudo-crossbar array structures to implement in-memory computing and accelerate the energy-efficient deep neural network training [14]. However, there are limitations for all these technologies. For example, RRAM may suffer from limited dynamic range (and thus lower on/off ratio), higher power consumption due to current-driven programming and filament-based conduction mechanism and low linearity. Fe-FET may provide higher on/off ratio, lower current for programming and higher dynamic range but a 2T cell is needed including a selector leading to a lower cell density. Therefore, looking for new synaptic devices with new materials, new structures and new physics is in strong demands.

In this work, we demonstrate a novel two-terminal memristor with metal-ferroelectric semiconductor-metal (M-FS-M) planar or crossbar structures for synaptic devices, which we coined as FSJ. Using FSJ as a synaptic device has two important advantages over the conventional FTJ or filament-based RRAM. First, the FSJ does not require ultra-thin ferroelectric film due to the semiconducting nature of the ferroelectric semiconductor. As is well-known, ferroelectricity in atomic scale is extremely difficult to retain due to the depolarization field. "Thicker" ferroelectric insulator in FTJ doesn't provide enough tunneling current. On the other hand, the conductance of FSJ can scale with the area so that it provides much more energy efficiency comparing with filament-based RRAM in scaled devices, because the resistive switching in FSJ is due to the ferroelectric polarization induced Schottky barrier height change.

Experimentally, α-In_2Se_3 based c-FSJ as a synaptic device is demonstrated. α-In_2Se_3 is a recently discovered ferroelectric semiconductor with a bandgap of ~1.39 eV, room temperature ferroelectricity, the ability to maintain ferroelectricity down to a few atomic layers [15-20]. α-In_2Se_3 ferroelectric semiconductor field-effect transistors (FeS-FETs) have been demonstrated showing high performance with high on/off ratio, large memory window and scaled supply voltage, suggesting ferroelectric semiconductor as a promising novel functional material for non-volatile memory applications [21]. Meanwhile, α-In_2Se_3 as a ferroelectric semiconductor also exhibits two-terminal ferroelectric resistive switching behavior [17, 19, 20]. Here, α-In_2Se_3 based c-FSJ as a synaptic device is demonstrated for the first time. Ferroelectric resistive switching is clearly observed in both p-FSJ by in-plane polarization switching and c-FSJ by out-of-plane polarization switching. Conductance potentiation and depression in the c-FSJ are measured and benchmarked at both original size and projected to 32 nm node with different synaptic devices, showing a good on-line learning accuracy of ~92%, low latency and energy consumption.

II. Experimental

α-In_2Se_3 bulk crystals were grown by chemical vapor transport (CVT). Fig. 1 shows the schematic diagram of an α-In_2Se_3 FeS-FET. The α-In_2Se_3 FeS-FET consists a heavily p-doped Si substrate as back-gate electrode, 30 nm HfO_2 as the gate dielectric, α-In_2Se_3 as channel material and 20 nm Ti/50 nm Au as source/drain electrodes. The device fabrication process is similar to the authors' previous work in [21]. If applying only source and drain two terminals, it is used as a p-FSJ, as shown in Fig. 2(a). Fig. 2(b) illustrates the M-FS-M crossbar structure as the c-FSJ. Ni is used for both bottom and top electrodes. Fig. 3 and Fig. 4 show top-view false-color SEM images of p-FSJ and c-FSJ structures, respectively. High-angle annular dark field STEM image and the corresponding selected area electron diffraction (SAED) of α-In_2Se_3 is shown in Fig. 5, showing a distinct arrangement of atoms and a highly single-crystalline hexagonal structure. Fig. 6 shows a photo image on the atomic layer thin single crystalline α-In_2Se_3 thin films directly grown on SiO_2 by chemical vapor deposition (CVD), suggesting a clear route for future large-area fabrication and integration. Material characterizations on α-In_2Se_3 crystals were carried out to investigate α-In_2Se_3 as a semiconducting and ferroelectric material, including photoluminescence (PL), Raman spectroscopy, and piezo force microscopy (PFM) [21]. All

electrical measurements were performed at room temperature and in dark condition.

III. Results and Discussion

Fig. 7 shows a PL spectrum of the bulk α-In_2Se_3 crystal, measured from 1.2 eV to 1.6 eV, indicating a direct bandgap of ~1.39 eV. Fig. 8 shows a Raman spectrum taken from the bulk α-In_2Se_3 crystal, showing consistent peaks comparing to literature reports on α-In_2Se_3 [19]. PFM is also applied to investigate the piezoelectricity and ferroelectricity of α-In_2Se_3, as shown in the PFM phase ferroelectric hysteresis loop in Fig. 9(b). The physical origin of ferroelectricity in α-In_2Se_3 is because of the non-centrosymmetric structure, as shown in Fig. 9(a) [15]. The Se atoms in the middle has two stable states within each layer, with both lateral and vertical dipole moments [17]. Therefore, α-In_2Se_3 has a correlated ferroelectric polarization in both in-plane direction and out-of-plane direction.

As a result, there are totally three operation mechanisms in α-In_2Se_3 FeS-FET and FSJ, as shown in Fig. 10. (i) Using gate voltage to control the out-of-plane polarization in the FeS-FET structure. (ii) Using drain-to-source voltage (V_{DS}) to control the in-plane polarization in the planar structure as p-FSJ. (iii) Using voltage across the top and bottom electrodes to control the out-of-plane polarization in the c-FSJ structure, as shown in Fig. 10(b). For high density synaptic device integration, two-terminal structure is critical, so p-FSJ and c-FSJ are mainly discussed in this work, especially for the c-FSJ due to its highest density. For both p-FSJ and c-FSJ, the ferroelectric polarization can tune the height/width of Schottky barrier at the metal/semiconductor interface, leading to a resistive switching behavior in I-V characteristics, as illustrated in Fig. 11.

Fig. 12 shows the I_D-V_{GS} characteristics of an α-In_2Se_3 FeS-FET with 15.9 nm thick α-In_2Se_3 (T_{FE}) and 30 nm thick HfO_2 as gate insulator. The transfer curve exhibits a clear counterclockwise hysteresis loop, indicating the threshold voltage is tuned by ferroelectricity instead of charge trapping. Fig. 13 shows the I-V characteristics of an α-In_2Se_3 p-FSJ with T_{FE} of 57.5 nm and a floating gate. I-V characteristics are measured for 10 repeated cycles, where a clear and reliable resistive switching is observed, but with a relatively small on/off ratio. By applying a back-gate voltage, the on/off ratio of the resistive switching I-V curve can be further improved due to the carrier density modulation thus Schottky barrier width change by gate voltage. As shown in Fig. 14, on/off ratio over 10^3 can be achieved at V_{GS}=-4 V. Fig. 15 shows the I-V characteristics of an α-In_2Se_3 c-FSJ with T_{FE} of 120 nm, measured at a ±2.5 V voltage range. The I-V characteristics are measured for 5 repeated cycles, showing reliable ferroelectric resistive switching with a coercive voltage ~ 2 V. The estimated coercive electric field (E_C) for out-of-plane polarization is about 0.016 V/nm, assuming a linear band bending. Note that the actual band bending in α-In_2Se_3 may be different due to the semiconducting nature. Fig. 16 shows the I-V characteristics of the same α-In_2Se_3 c-FSJ measured at a ±2 V voltage range below the coercive electric field, exhibiting a negligible hysteresis without ferroelectric switch of α-In_2Se_3.

Fig. 17 illustrates the potentiation and depression pulse measurements. Identical pulses are used with positive pulses for potentiation and negative pulses for depression, where the conductance of the c-FSJ is sampled after each pulse at 0.5 V below the coercive voltage. Fig. 18 shows the experimental potentiation and depression profiles for a representative c-FSJ device with different pulse width from 80 ns to 150 ns. +2 V is used for potentiation and -2 V is used for depression. ±2 V is above the coercive field since the measured c-FSJ here has T_{FE} of 70 nm. The nonlinearity of the potentiation and depression process is extracted by fitting to the experiments using the model reported in [14], as shown in Fig. 19. Fig. 20 shows the extracted nonlinearity (α_p for potentiation and α_d for depression). An improved nonlinearity is achieved with smaller pulse width. The best nonlinearity achieved at 80 ns is α_p=4.22 and α_d=-4.22. The large nonlinearity can be improved by using non-identical pulses [12] and pulse condition optimization [13].

To benchmark the performance of the α-In_2Se_3 c-FSJ synaptic device, an MLP+NeuroSimv3.0 based training simulation is performed [14], where an adaptive momentum estimation training algorithm is adopted, as shown in the training process in Fig. 21. Fig. 22 shows the benchmarking of α-In_2Se_3 c-FSJ synaptic device with various reported synaptic devices. α-In_2Se_3 c-FSJ shows good on-line learning accuracy at ~92%, lowest latency and energy consumption when projected to 32 nm node due to the short write pulse width (low latency) and large R_{ON} (low energy consumption), suggesting the α-In_2Se_3 c-FSJ is a promising and competitive synaptic device.

IV. Conclusion

In summary, we report on a novel crossbar FSJ based two-terminal memristor as a synaptic device for the first time. Ferroelectric semiconductor α-In_2Se_3 based planar and crossbar FSJs are experimental demonstrated showing clear resistive switching behavior. Conductance potentiation and depression in the c-FSJ are measured and benchmarked with various synaptic devices, showing advantage in accuracy, latency and energy consumption. FSJ provides the advantages in scalability and energy efficiency over the conventional RRAM and FTJ. FSJ is a promising and competitive synaptic device candidate for in-memory computing and deep neural network applications.

Acknowledgment

The work was supported in part by ASCENT, one of six centers in JUMP, a SRC program sponsored by DARPA. The work was also partly supported by AFOSR/NSF 2DARE program and ARO. The authors also acknowledge the technical support from J. Jian and H. Wang on TEM imaging and S. Gao and W. Wu on PFM measurements.

References

[1] S. Yu, Proc. IEEE, pp. 260-285, 2018. [2] X. Xia et al., Nat. Mater., vol. 18, pp. 309-323, 2019. [3] S. H. Jo et al. Nano Lett., vol. 10, pp. 1297-1301, 2010. [4] S. Park et al., IEDM 2013, pp. 625-628. [5] J. Woo et al., IEEE EDL, pp. 994-997, 2016 [6] W. Wu et al., VLSI 2018, pp. T103-T104. [7] M. Suri et al., IEDM 2011, pp. 79-82. [8] D. Kuzum et al., Nano Lett., vol. 12, 2179-2186, 2012. [9] G. W. Burr et al., IEEE TED, vol. 62, pp. 3498-3507, 2015. [10] A. Chanthbouala et al., Nat. Mater., vol. 11, pp. 860-864, 2012. [11] H. Mulaosmanovic et al., VLSI 2017, pp. T176–T177. [12] M. Jerry et al., in IEDM 2017, pp. 139-142, 2017. [13] W. Chung et al., IEDM 2018, pp. 344-347. [14] P. Y. Chen et al., IEDM 2017, pp. 135-138. [15] Y. Zhou et al., Nano Lett., vol. 17, pp. 5508-5513, 2017. [16] W. Ding et al., Nat. Commun., vol. 8, p. 14956, 2017. [17] C. Cui et al., Nano Lett., vol. 18, pp. 1253-1258, 2017. [18] J. Xiao et al., Phys. Rev. Lett., vol. 120, p. 227601, 2018. [19] S. Wan et al., Nanoscale, vol. 10, pp. 14885-14892, 2018. [20] F. Xue et al., Adv. Mater., p. 1901300, 2019. [21] M. Si et al., arXiv:1812.02933, 2018.

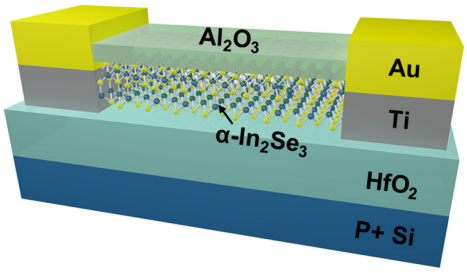

Fig. 1. Schematic diagram of an α-In_2Se_3 FeS-FET.

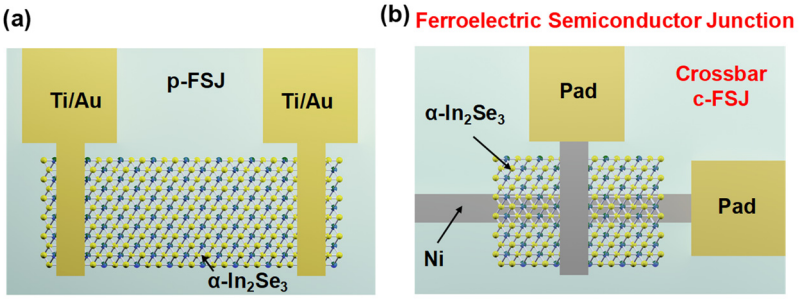

Fig. 2. Top-view schematic diagrams of (a) a planar ferroelectric semiconductor junction (p-FSJ) and (b) a crossbar ferroelectric semiconductor junction (c-FSJ).

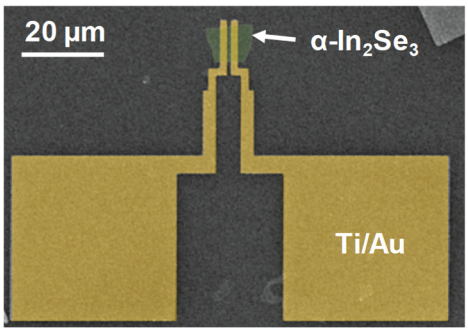

Fig. 3. Top-view false-color SEM image of a fabricated α-In_2Se_3 FeS-FET or p-FSJ.

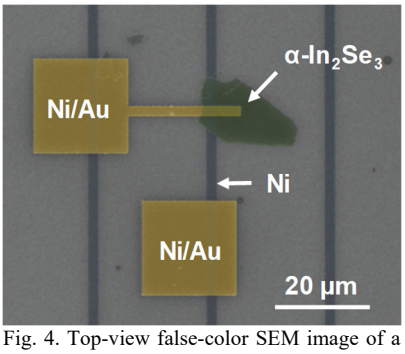

Fig. 4. Top-view false-color SEM image of a fabricated α-In_2Se_3 c-FSJ.

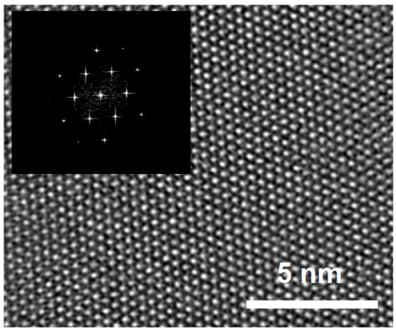

Fig. 5. STEM image and the corresponding SAED image of a thin α-In_2Se_3 film.

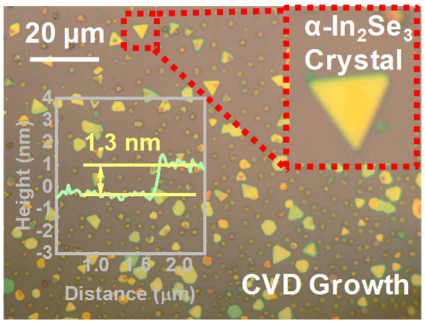

Fig. 6. CVD growth of α-In_2Se_3 single-crystal ultrathin films on SiO_2 surface. The films can be as thin as mono-layer as shown by the inset AFM image.

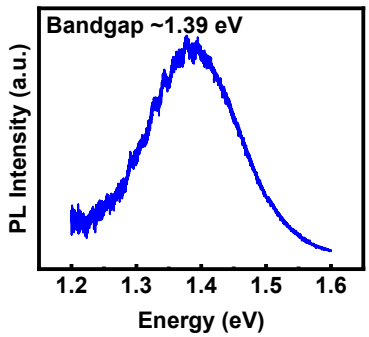

Fig. 7. Photoluminescence spectrum of bulk α-In_2Se_3 at room temperature, showing a bandgap of ~1.39 eV without considering 2D exciton binding energy.

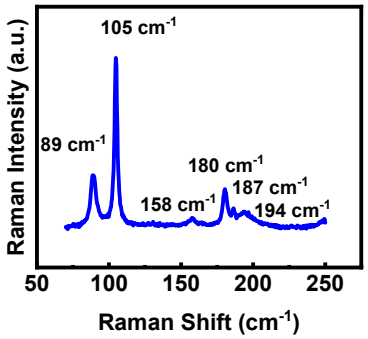

Fig. 8. Raman spectrum of bulk α-In_2Se_3 at room temperature.

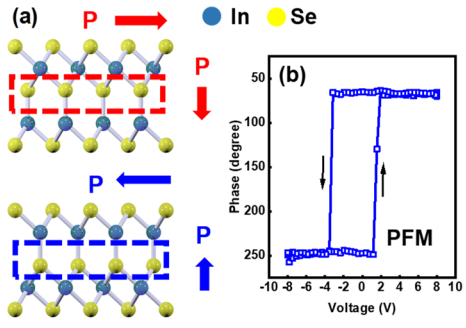

Fig. 9. (a) Atomic structure and the origin of in-plane and out-of-plane polarization in ferroelectric α-In_2Se_3. (b) PFM measurement of phase vs. voltage ferroelectric hysteresis loop.

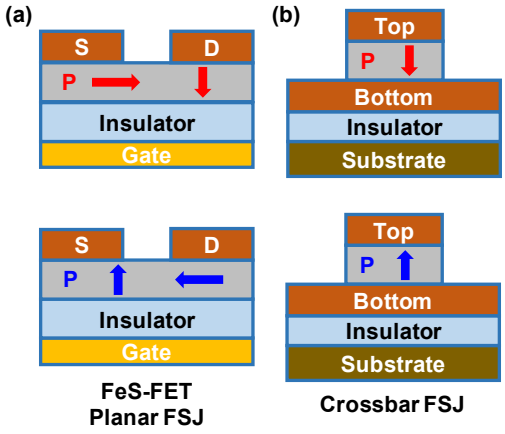

Fig. 10. Control of polarization in ferroelectric semiconductor α-In_2Se_3 in (a) FeS-FET or p-FSJ and (b) c-FSJ.

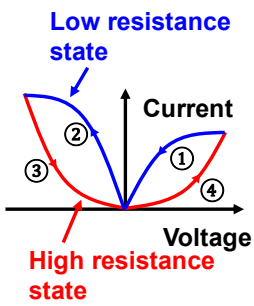

Fig. 11. Illustration of resistive switching due to different polarization direction in ferroelectric semiconductor α-In_2Se_3.

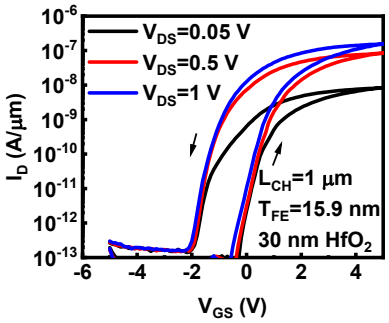

Fig. 12. I_D-V_{GS} characteristics of an α-In_2Se_3 FeS-FET with 1 μm channel length, 15.9 nm channel thickness and 30 nm HfO_2 as gate insulator.

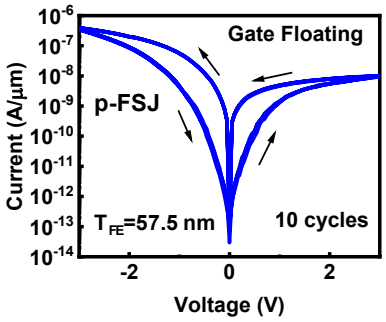

Fig. 13. I-V characteristics of an α-In_2Se_3 p-FSJ with gate floating and channel length of 1 μm. Resistive switching is controlled by in-plane ferroelectric polarization.

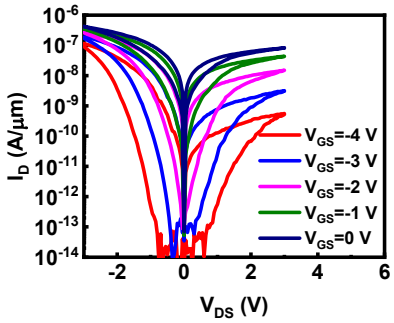

Fig. 14. I-V characteristics of the same α-In_2Se_3 p-FSJ as in Fig. 13, with different gate voltages.

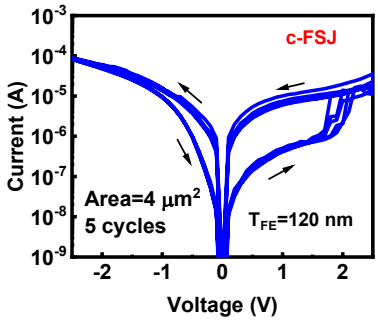

Fig. 15. I-V characteristics of an α-In_2Se_3 c-FSJ at ±2.5 V range. Resistive switching is controlled by out-of-plane ferroelectric polarization.

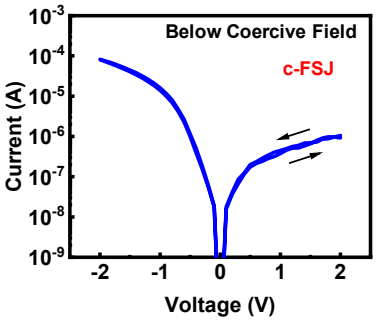

Fig. 16. I-V characteristics of the same α-In_2Se_3 c-FSJ as in Fig. 15 at ±2 V range below the coercive electric field. No resistive switching phenomenon is observed.

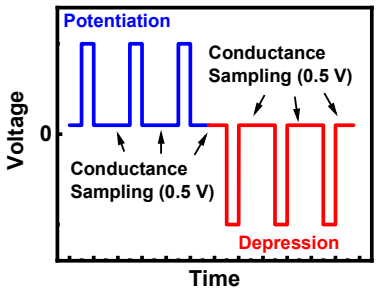

Fig. 17. Illustration of pulse sequence for potentiation and depression measurements.

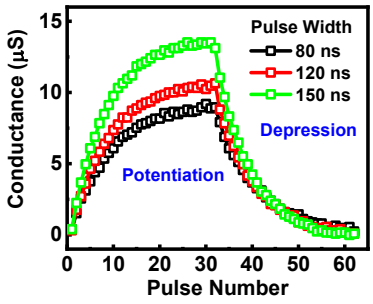

Fig. 18. Potentiation and depression profile with different pulse width. +2 V is used for potentiation and -2 V is used for depression. The current is measured at 0.5 V. T_{FE} is 70 nm so that ±2 V is above the coercive voltage.

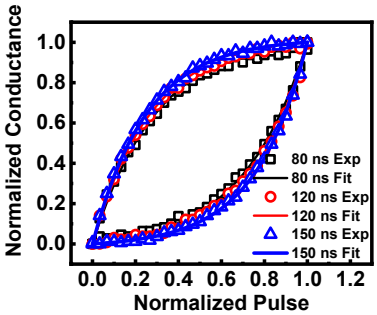

Fig. 19. Normalized conductance versus normalized pulse number for the fitting of nonlinearity.

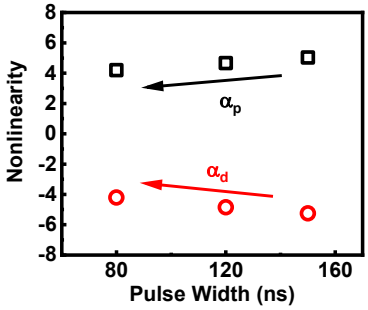

Fig. 20. Nonlinearity extracted by fitting to experimental results for different pulse widths.

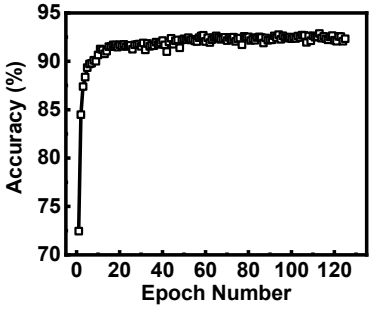

Fig. 21. Accuracy versus epoch number in the training simulation (80 ns pulse width) based on MLP+NeuroSimv3.0.

Device type	Ag:a-Si [3]	TaO_x/HfO_x [6]	PCMO [4]	AlOx/HfO_2 [5]	α-In_2Se_3 c-FSJ (original size) This work	α-In_2Se_3 c-FSJ (projected to 32nm) This work
# of conductance states	97	128	50	40	31	31
Nonlinearity (α_p/α_d)	2.4/-4.88	0.04/-0.63	3.68/-6.76	1.94/-0.61	4.22/-4.22	4.22/-4.22
R_{ON}	26MΩ	100KΩ	23MΩ	16.9KΩ	100KΩ	390MΩ
ON/OFF ratio	12.5	10	6.84	4.43	21	21
Weight increase pulse	3.2V/300μs	1.6V/50ns	2V/1ms	0.9V/100μs	2V/80ns	2V/80ns
Weight decrease pulse	-2.8V/300μs	-1.6V/50ns	-2V/1ms	-1V/100μs	-2V/80ns	-2V/80ns
Cycle-to-cycle variation (σ)	3.5%	3.7%	<1%	5%	<0.5%	<0.5%
Online learning accuracy	~90%	~92%	~90%	~91%	~92%	~92%
Area	6292.3μm²	8663.1μm²	6292.3μm²	21,846μm²	184,420μm²	6292.3μm²
Latency (optimized)	22,402s	6.1s	16,545s	679s	0.81s	1.04s
Energy (optimized)	10.9mJ	2.2mJ	3.5mJ	26.1mJ	3.09mJ	1.53mJ
Leakage power	105.6μW	105.6μW	105.6μW	105.6μW	105.6μW	105.6μW

Fig. 22. Benchmarking of various synaptic devices. α-In_2Se_3 c-FSJ exhibits low energy consumption, low latency and high accuracy.